AIP | Journal of Applied Physics

A self-consistent global model of solenoidal-type inductively coupled plasma discharges including the effects of radio-frequency bias power

D. C. Kwon, W. S. Chang, M. Park, D. H. You, M. Y. Song et al.

Citation: J. Appl. Phys. **109**, 073311 (2011); doi: 10.1063/1.3572264
View online: http://dx.doi.org/10.1063/1.3572264
View Table of Contents: http://jap.aip.org/resource/1/JAPIAU/v109/i7
Published by the American Institute of Physics.

A self-consistent global model of solenoidal-type inductively coupled plasma discharges including the effects of radio-frequency bias power

D. C. Kwon,[1,a)] W. S. Chang,[1] M. Park,[2] D. H. You,[3] M. Y. Song,[1] S. J. You,[4] Y. H. Im,[5] and J.-S. Yoon[1]
[1]*Convergence Plasma Research Center, National Fusion Research Institute, Daejeon 305-333, Korea*
[2]*Department of Physics, Korea Advanced Institute of Science and Technology, Daejeon 305-701, Korea*
[3]*Kyoungwon Tech, Inc., Seongnam 462-806, Korea*
[4]*Center for Vacuum Technology, Korea Research Institute of Standard and Science, Daejeon 305-340, Korea*
[5]*Division of Chemical Engineering, Chonbuk National University, Jeonju 561-756, Korea*

(Received 14 December 2010; accepted 3 March 2011; published online 11 April 2011)

We developed a self-consistent global simulator of solenoidal-type inductively coupled plasma discharges and observed the effect of the radio-frequency (rf) bias power on the plasma density and the electron temperature. We numerically solved a set of spatially averaged fluid equations for charged particles, neutrals, and radicals. Absorbed power by electrons is determined by using an analytic electron heating model including the anomalous skin effect. To analyze the effects of rf bias power on the plasma properties, our model also combines the electron heating and global transport modules with an rf sheath module in a self-consistent manner. The simulation results are compared with numerical results by using the commercial software package CFD-ACE+ (ESI group) and experimental measurements by using a wave cutoff probe and a single Langmuir probe. © *2011 American Institute of Physics*. [doi:10.1063/1.3572264]

I. INTRODUCTION

Inductively coupled plasma (ICP) sources are widely used in semiconductor fabrication processing because a high density plasma with good uniformity is easily obtained under low pressure without an external magnetic field.[1–4] Moreover, compared to other reactors (Helicon, ECR, etc.), the ICP reactor can be easily scaled up to accommodate a large wafer size because the system is substantially simpler.[5,6] Accordingly, many research groups have been researching the ICP reactor, and it is already being applied to a partial semiconductor manufacturing line.

In the modeling of plasma etching equipment that have radio-frequency (rf) biased on a substrate, the rf sheath must be accurately represented to properly simulate the ambipolar fields, the electron stochastic heating, and a self-bias. Lieberman[7,8] derived analytical solutions assuming a sinusoidal current source, and Godyak and Stemberg[9,10] have done extensive modeling. Miller and Riley[11] presented the unified sheath model, and Panagopoulos and Economou[12] obtained an analytic expression for the energy split of the ion energy distributions arriving at the substrates based on the work of Miller and Riley. Edelberg *et al.*[13] determined the ion energy distributions (IEDs) by using a self-consistent dynamic model of the rf sheath by coupling an equivalent circuit model to the fluid equation. Bose *et al.*[14] solved the fluid equation assuming a sinusoidal voltage source including the inertial term in the ion momentum equation. Later, Dai *et al.*[15] proposed a self-consistent fluid model that included all time-dependent terms in the ion fluid equations and assumed the sinusoidal current source.

However, numerically resolving the thin sheath in computer models of the devices requires large computing resources. Therefore, based on the Miller and Riley's semianalytical solution for rf sheath, Grapperhaus and Kushner[16] developed a sheath model that is solved self-consistently within the framework of a two-dimensional hybrid plasma equipment model (HPEM). The sheath model consists of a one-dimensional local model that is implemented at each mesh point at the boundary of the plasma and the walls of the reactor. Although the authors of Ref. 16 combined the transport module with the rf sheath module, only voltage source condition on the substrate is adopted in their model, and they did not fully investigate the effects of rf bias power on the plasma parameters.

In a recent study, the changes of the electron temperature and the plasma density by increasing bias power were observed in planar-type ICP discharges.[17] The authors of Ref. 17 explained the changes of the plasma parameters by using the balance between total power absorption and power dissipation. However, the absorbed source and bias powers and the total loss energy at the grounded wall and the substrate should be determined in a self-consistent manner.

Therefore, in this work, we solve a set of spatially averaged global fluid equations for charged particles, neutrals, and radicals.[18,19] Absorbed power by electrons is determined by using an analytic electron heating model including the anomalous skin effect.[3] Our model combines the electron heating and global transport modules with an rf sheath module in a self-consistent manner based on the recently developed Dai's model.[15] Although the Dai's model is the self-consistent fluid model, we found that the self-bias under most conditions were obtained in seconds. The simulation results are compared with experimental measurements by using a wave cutoff probe[20,21] and a single Langmuir

a)Author to whom correspondence should be addressed. Electronic mail: dckwon@nfri.re.kr.

probe.[22,23] We also performed the two-dimensional fluid simulation by using the commercial software package CFD-ACE + (ESI group).[24]

Unfortunately, in CFD-ACE +, only the sinusoidal voltage source boundary conditions can be applied for rf bias. Assuming the sinusoidal voltage source, we also use a simple circuit model based on the previously developed model. Kim *et al.*[4] determined the dc self-bias by using a circuit model[25] from the plasma parameters. They regarded sheaths on the chamber wall and biased substrate as capacitors, and the capacitors are connected in series through plasma. In their model, the capacitively coupling between antenna and plasma is not considered. In a similar manner, we use an equivalent circuit model and expand their model based on the unified rf sheath model.[11,12] The obtained amplitude of applied rf voltage is used for voltage boundary conditions of the two-dimensional fluid model.

This paper is organized as follows: In Sec. II, the electron heating model, spatially averaged global fluid equations, and rf sheath model are explained. The experimental apparatus is described in Sec. III. Then the numerical and experimental results are presented in Sec. IV. Finally, the conclusion is given in Sec. V.

II. MODEL DESCRIPTIONS

A schematic diagram of the solenoidal-type ICP reactor is shown in Fig. 1. The power absorbed by electrons, including the anomalous skin effect, is calculated by the heating module. The resulting power absorbed by electrons is used to calculate the plasma density and electron temperature in the plasma transport module. The plasma transport module then returns the plasma density and electron temperature to the rf sheath module. Then the sheath voltage drop is obtained from the rf sheath module, which is coupled with the transport module in a self-consistent manner. These processes are repeated until a self-consistent steady state is obtained (see Fig. 2). The detailed models used in this work are described in the following text subsections.

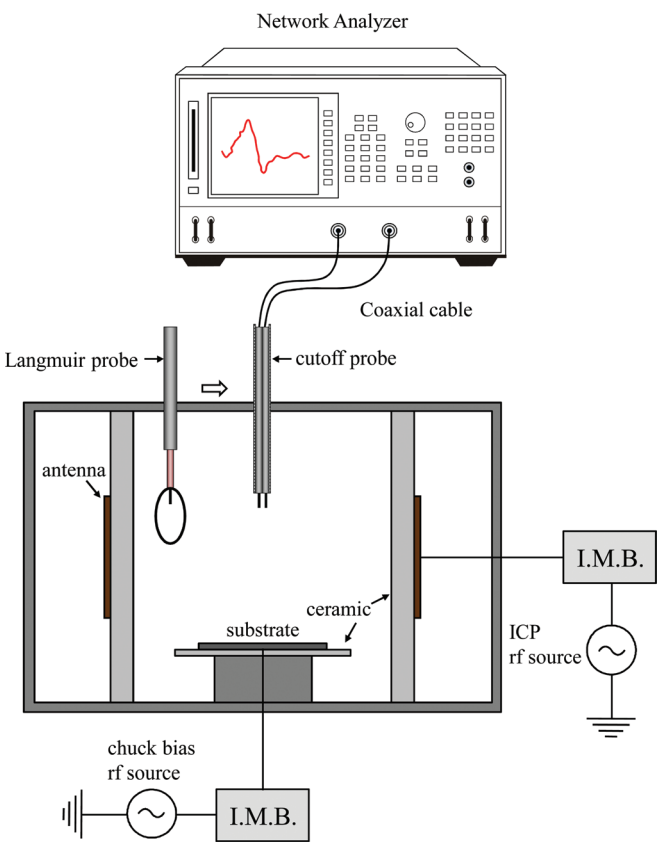

FIG. 1. (Color online) A schematic diagram of the solenoidal-type ICP reactor.

A. Electron heating model

To determine the power absorbed by electrons, we used the previously developed analytic heating model based on collisionless nonlocal electron heating.[3]

Assuming θ-symmetry, the wave equation describing the inductive electric field component having only a θ component becomes

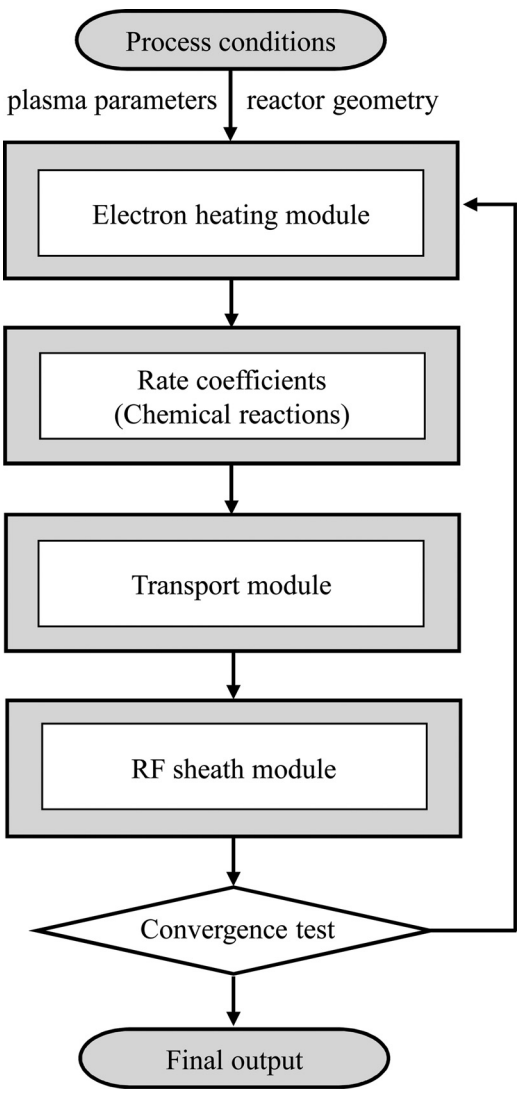

FIG. 2. A block diagram of the simulation modules.

TABLE I. Gas-phase reactions included in simulations of Ar plasma and their rate coefficients.

Reactions	A	B	C	ΔE	Reference
Electron-impact reactions					
$e + Ar \rightarrow Ar^* + e$	2.783×10^{-16}	0.3287	140200.0	11.6	26
$e + Ar \rightarrow Ar^+ + 2e$	5.779×10^{-17}	0.6329	186400.0	15.76	27
$e + Ar^* \rightarrow Ar^+ + 2e$	6.225×10^{-14}	0.1072	51210.0	4.43	28
$e + Ar^* \rightarrow Ar + e$	2.645×10^{-16}	0.2894	8601.0	− 11.6	26[a]
Metastable reactions					
$Ar^* + Ar^* \rightarrow Ar^+ + Ar + e$	1.200×10^{-15}	0.0000	0.0		29

The rate coefficients are in the form $k_j = A_j T_e^{B_j} \exp(-C_j/T_e)$. The units of k_j are in $m^3 s^{-1}$ and T_e is in Kelvin.
[a]Cross-section was obtained by detailed balance.

$$\frac{\partial^2 E_\theta}{\partial r^2} + \frac{1}{r}\frac{\partial E_\theta}{\partial r} - \frac{E_\theta}{r^2} + \frac{\partial^2 E_\theta}{\partial z^2} + \mu_0 \varepsilon_0 \omega^2 E_\theta = -\mu_0 \omega i (J_c + J_p), \tag{1}$$

where μ_0 is the permeability of free space, ε_0 is the permittivity of free space, ω is the excitation frequency, and J_c and J_p represent the antenna and plasma current densities, respectively. Assuming that the whole chamber wall is surrounded with a perfect conductor, You *et al.* obtained the electromagnetic fields by using the mode excitation method, including the anomalous skin effect.[3] Using the obtained analytic electromagnetic fields, a tractable form of the plasma resistance was obtained as a function of various plasma and geometrical parameters.

Then the power absorbed by electrons is given by

$$P_{abs} = \frac{R_p}{R_p + R_c} P_{rf}, \tag{2}$$

where R_p is the plasma resistance, R_c is the antenna resistance, and P_{rf} is the rf power supplied at the powered antenna.[19]

B. Global transport model

We numerically solve the spatially averaged continuity equation and electron temperature equation based on the Ar plasma chemistry[26–29] as shown in Table I. The rate coefficients for the electron impact reactions listed in Table I were calculated by assuming that the electron energy distribution function is Maxwellian. The values of the rate coefficients were fit using the Arrhenius form; we chose the fitting parameters such that the match was best for electron temperatures in the range of 1-7 eV.

The governing equations[18,19] of the spatially averaged global model are as follows:

$$\frac{\partial n_i}{\partial t} = \sum_j k_{ij} n_e n_j + \sum_{j,k} k_{ijk} n_j n_k + Q_{inlet} - n_i \left(\sum_j k_{ji} n_e + \sum_{i,k} k_{jik} n_k \right) - n_i v_l^i - Q_{pump}, \tag{3}$$

$$\frac{\partial}{\partial t}\left(\frac{3}{2} n_e T_e\right) = \frac{P_{abs}}{\Omega} - E_e - n_e \varepsilon_{e,l} v_l^e, \tag{4}$$

where n_i is the density of species i particle. k_{ij} is the electron impact rate coefficient of species i generation by electron collision with species j and k_{ijk} is the rate coefficient of species i generation by reactions between species j and k. Q_{inlet} and Q_{pump} are the source and loss terms by gas inlet and pumping out, respectively. n_e is the electron density, T_e is the electron temperature, Ω is the volume of the chamber, and E_e is the collisional energy loss term.

The loss speed of the ions at the plasma-sheath boundary is assumed to be the Bohm velocity, and, thus the loss frequency of the ith ion species becomes $v_l^i = S_e \sqrt{T_e/M_i}/\Omega$. Here, S_e is the effective area for particle loss and M_i is the ion mass. Assuming the ambipolar diffusion, the loss frequency of the escaping electron into the wall is given by $v_l^e = \sum_i S_e \sqrt{T_e/M_i}/\Omega$.[18,19]

Equation (4) is the spatially averaged electron temperature equation. The equation and the loss energy $\varepsilon_{e,l}$ into the wall can be directly derived from integrating the below electron temperature equation over space.

$$\frac{\partial}{\partial t}\left(\frac{3}{2} n_e' T_e'\right) = -\nabla \cdot Q_e - eE \cdot \Gamma_e + P_{abs}' - E_e', \tag{5}$$

where n_e', T_e', P_{abs}', and E_e' are the local electron density, the local electron temperature, the local power absorption, and the local collisonal energy loss term, respectively. Q_e is the electron energy flux, E is the electric field, and Γ_e is the electron flux. If Eq. (5) is divided by the volume of the chamber and integrated over space, we have

$$\frac{\partial}{\partial t}\left(\frac{3}{2} n_e T_e\right) = \frac{P_{abs}}{\Omega} - E_e - \frac{1}{\Omega}\int (\nabla \cdot Q_e + e\mathbf{E} \cdot \Gamma_e)\, d\tau. \tag{6}$$

Assuming the isothermal thin sheath and the force balance condition of massless electron, the third term on the right-hand side of Eq. (6) can be rewritten as

$$\frac{1}{\Omega}\int (\nabla \cdot Q_e + e\mathbf{E} \cdot \Gamma_e)\, d\tau \cong \frac{S_e}{\Omega}\frac{5}{2}\Gamma_{e,w} T_{e,w} + e\frac{S_e}{\Omega}\Gamma_{e,w} V_{sh} \equiv n_e \varepsilon_{e,1} v_1^e, \tag{7}$$

where V_{sh} is the sheath potential drop, and $\Gamma_{e,w}$ and $T_{e,w}$ are the electron flux and electron temperature at the wall, respectively. Thus we can define the loss energy into the wall as $\varepsilon_{e,1} = V_{sh} + 2.5T_e$.

If the bias power is applied to the substrate, $\varepsilon_{e,1}$ can be given by

$$\varepsilon_{e,1} \cong \frac{1}{n_e u_B}\left\langle \int_{\text{edge}}^{\text{wall}} \left(-e\frac{\partial V}{\partial z}\Gamma_e\right) dz \right\rangle + 2.5T_e. \quad (8)$$

Here we assume that the sheath is uniform in radial direction. Thus the sheath potential drop can be obtained by integrating the first term on the right-hand side of Eq. (8) from the sheath edge to the wall. To simplify the analysis, we assume that the electron current density is uniform within the thin sheath. Finally, we have

$$V_{sh} = \begin{cases} V_p & \text{at the chamber wall,} \\ V_p - \langle V_s \rangle & \text{at the substrate.} \end{cases}$$

Here $\langle V_s \rangle$ is the time averaged voltage on the substrate. $\langle V_s \rangle$ is obtained from the rf sheath module that is coupled with the transport module in a self-consistent manner.

C. Rf sheath model

To determine the bias voltage from the plasma parameters, in this work, we use not only the Dai's model but also a circuit model as shown in Fig. 3.

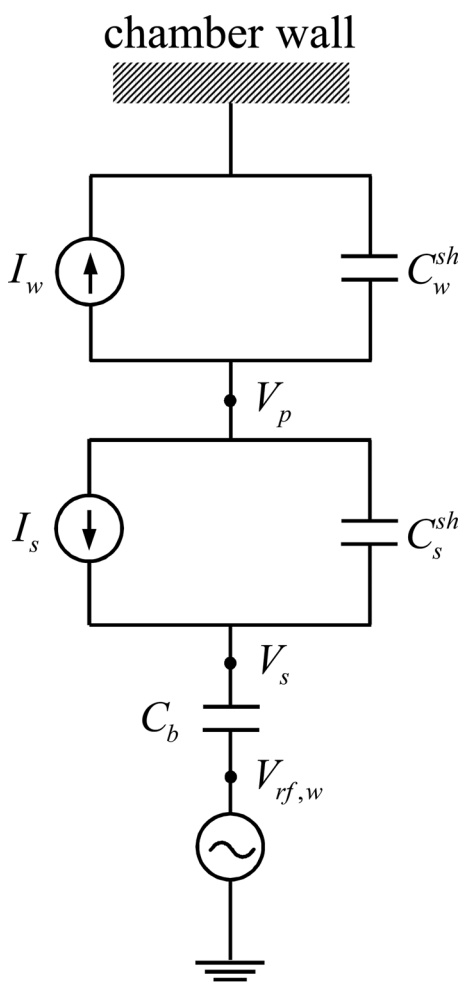

FIG. 3. Schematic diagram of equivalent circuit for rf sheath model.

We assume that the time averaged power flowing from the rf bias power into the discharge is totally absorbed within the sheath region because the impedance of the bulk plasma is quite small comparing the sheath impedance for the high-density and low-pressure plasmas. Therefore, the rf bias power to the substrate can be calculated from the time dependent voltage and current wave forms as

$$P'_{\text{bias}} = \frac{1}{\tau}\int_0^\tau V_s(t)\, I_s(t)\, dt, \quad (9)$$

where $\tau = 2\pi/\omega$ is the rf cycle and $I_s(t)$ is the current on the substrate. Until P'_{bias} becomes equal to the applied rf bias power of P_{bias} within the margin of error, the amplitude of applied rf current or voltage is determined by Eq. (9) with an iterative process. The obtained amplitude of applied rf voltage is also used for voltage boundary conditions of a two-dimensional fluid model.

1. Current control model (Model I)

The one-dimensional spatiotemporal variations of ion density, electron density, ion velocity, and electric potential are described by the ion continuity equation, the Boltzmann relation, the momentum equation, and the Poisson's equation, respectively:[15]

$$\frac{\partial n_i}{\partial t} + \frac{\partial (n_i u_i)}{\partial x} = 0, \quad (10)$$

$$\frac{\partial u_i}{\partial t} + u_i \frac{\partial u_i}{\partial x} = -\frac{e}{M_i}\frac{\partial V}{\partial x}, \quad (11)$$

$$n_e = n_s \exp\left(\frac{eV}{T_e}\right), \quad (12)$$

$$\frac{\partial^2 V}{\partial x^2} = -\frac{e}{\varepsilon_0}(n_i - n_e), \quad (13)$$

where u_i is the velocity of ion species, e is the elementary charge, V is the potential, and $n_s = n_0 \exp(eV_1/T_e)$. Here, $V_1 = -T_e/2e$ denotes the potential drop in the presheath, and n_0 is the plasma density.[25]

Assuming a sinusoidal current source at the electrode, a current balance can be written as $J_i + J_e + J_d = J_0 \sin(2\pi ft)$, where J_i and J_e are the conduction current densities of the ion and electron, respectively.[12,13,15] The displacement current density, J_d, can be derived as

$$J_d \equiv \frac{C_s(t)}{A}\frac{dV_s(t)}{dt} - \frac{V_s(t)}{A}\frac{dC_s(t)}{dt}, \quad (14)$$

where $C_s(t)$ is the sheath capacitance and A is the surface area of the substrate.[15] The current balance is coupled to the sheath model through the electrode potential and the sheath thickness. By solving the current balance equation with the fourth order Runge–Kutta method, we obtain the potential drop across the sheath. Using the obtained potential $V_s(t)$, we then solve the fluid equations and the Poission's equation by using a finite difference method with an iterative process.

Assuming that the current at the electrode from the rf bias supply is sinusoidal, Eq. (9) can be rewritten as

$P'_{\text{bias}} = 1/\tau \int_0^\tau V_s(t)\, I_{\max} \sin(\omega t)\, dt$, where $I_{\max}$ is the amplitude of applied rf bias current.

2. Voltage control model (Model II)

As mentioned in the preceding text, numerically resolving the thin sheath in computer models of the devices requires large computing resources. To reduce the computing resources and compare the our results with the two-dimensional fluid model, we also use a simple circuit model based on the previously developed model.[4,11,25] The schematic diagram of an equivalent circuit is described in Fig. 3. Based on the previously developed rf sheath model, the following circuit relations can be obtained.

$$C_s^{sh} \frac{\partial}{\partial t}(V_p - V_s) + I_s + C_b \frac{\partial}{\partial t}(V_{rf} - V_s) = 0, \tag{15}$$

$$C_w^{sh} \frac{\partial V_p}{\partial t} + I_w + C_s^{sh} \frac{\partial}{\partial t}(V_p - V_s) + I_s = 0, \tag{16}$$

$$\frac{\partial \bar{V}_s}{\partial t} = \frac{\partial V_p}{\partial t} - \omega_{pi}(\bar{V}_s - V_s), \tag{17}$$

$$\frac{\partial \bar{V}_w}{\partial t} = \frac{\partial V_p}{\partial t} - \omega_{pi}\bar{V}_w, \tag{18}$$

where $\bar{V}_s$ and $\bar{V}_w$ are damped potential at the substrate and chamber wall, respectively. C_s^{sh} and C_w^{sh} are the sheath capacitance on the substrate and chamber wall, respectively, C_b is the blocking capacitance, and $\omega_{pi} = \sqrt{e^2 n_s/\varepsilon_0 M_i}$. The sheath capacitance C^{sh} is related to voltage drop across the sheath as $C^{sh} = A\varepsilon_0 \partial E/\partial V_{sh}$,[11,12] where

$$\frac{\partial E}{\partial V_{sh}} = \frac{e n_s T_e}{\varepsilon_0 E}\left\{\frac{M^2}{\bar{V}_{sh}}\left[\sqrt{1 - \frac{2\bar{V}_{sh}}{M^2 T_e}} - 1\right] + \frac{1}{T_e}\exp\left(\frac{V_{sh}}{T_e}\right)\right\}. \tag{19}$$

Here, $V_{sh} = V_s(\text{or } V_w) - V_p$, $\bar{V}_{sh} = \bar{V}_s(\text{or}\bar{V}_w) - V_p$, M is the Mach number, and the electric field is

$$E = -\left(E_s^2 + \frac{2 e n_s T_e}{\varepsilon_0}\left\{\frac{M^2 V_{sh}}{\bar{V}_{sh}}\left[\sqrt{1 - \frac{2\bar{V}_{sh}}{M^2 T_e}} - 1\right] + \left[\exp\left(\frac{V_{sh}}{T_e}\right) - 1\right]\right\}\right)^{1/2}, \tag{20}$$

where the electric field at the sheath-presheath boundary is $E_s = -T_e \log(\varepsilon)/\lambda_i$.[11,12] ε is the ratio of the electron Debye length to the ion mean free path. The total current I to the sheath can be given by $I = A(J_i + J_e) - \bar{C}^{sh}\partial \bar{V}_{sh}/\partial t$, where $\bar{C}^{sh} = A\varepsilon_0 \partial E/\partial \bar{V}_{sh}$. Here,

$$\frac{\partial E}{\partial \bar{V}_{sh}} = \frac{e n_s T_e}{\varepsilon_0 E}\frac{M^2 V_{sh}}{\bar{V}_{sh}^2}\left\{1 - \sqrt{1 - \frac{2\bar{V}_{sh}}{M^2 T_e}} - \frac{\bar{V}_{sh}/M^2 T_e}{\sqrt{1 - 2\bar{V}_{sh}/M^2 T_e}}\right\}. \tag{21}$$

Assuming that the voltage at the electrode from the rf bias supply is sinusoidal, Eq. (9) can be rewritten as $P'_{\text{bias}} = 1/\tau \int_0^\tau V_{\max} \sin(\omega t)\, I_s(t)\, dt$, where $V_{\max}$ is the amplitude of applied rf bias voltage.

III. EXPERIMENT

To validate our model, the experiments were performed at an ICP reactor of Surface Technology Systems (STS) as shown in Fig. 1. The single-turned antenna coil (radius: 0.1905 m, width: 0.001 m height: 0.05 m) is wound around the dielectric tube of which radius and height are 0.172 and 0.165 m, respectively. The Ar gas of 10 sccm is fed from the mass flow controller (MFC), the pressure is 20 mTorr, and the rf source power at 13.56 MHz was supplied to a rf antenna via L-type matching network.

In the present study, we used the cutoff probe for the precise measurement of the electron density.[20] It is well known that plasma density can be measured by using the cutoff probe within 2% of uncertainty.[21] The cutoff probe consisted of two tips as shown in Fig. 1. One was a microwave radiating antenna connected to the radiating port of a network analyzer through a 50 Ω coaxial cable, and the other was a detecting antenna connected to the receiving port of the network analyzer. The cutoff probe was mounted on a top plate center, and the plasma density was measured at the five different positions from 0.05 to 0.125 m in axial direction. The averaged values of the five points for the measured electron density were used to compare the simulation results. To acquire the electron temperature and the electron energy probability functions (EEPFs), the rf compensated single Langmuir probe (SLP2000) were used. The SLP was also mounted on a top plate center; we measured the electron temperature and EEPFs in axial direction.

IV. RESULTS

In Sec. II, we described the self-consistent global model, which consists of the heating module, plasma transport module, and rf sheath module. The simulation results are compared with not only experimental measurements by using the cutoff probe and the SLP but also two-dimensional numerical results by using the CFD-ACE +.

CFD-ACE + is suitable for modeling a variety of coupled physical phenomena, such as fluid dynamics, electrodynamics, heat, and complex chemical reactions. The governing equations used for the plasma simulation are the Navier Stokes and continuum equations for gas flow and heat transfer, nonequilibrium plasma transport, and species transport, and the Poisson equation for electrostatic field. Two-dimensional simulations were performed for Ar plasma (see Table I) under the same operating conditions and reactor geometry as used in the experiments.

Figure 4 shows the dependence of plasma densities on the bias power for various ICP source powers. Although there is a difference in the absolute values, as the bias power increases, we can see that the numerically solved plasma densities are in a good agreement with the measured results. Here, data numerically solved by using the two-dimensional fluid model were averaged in the same manner as with the experiments. Our results, both simulation and experience agree well with the previous report[17] that observed plasma

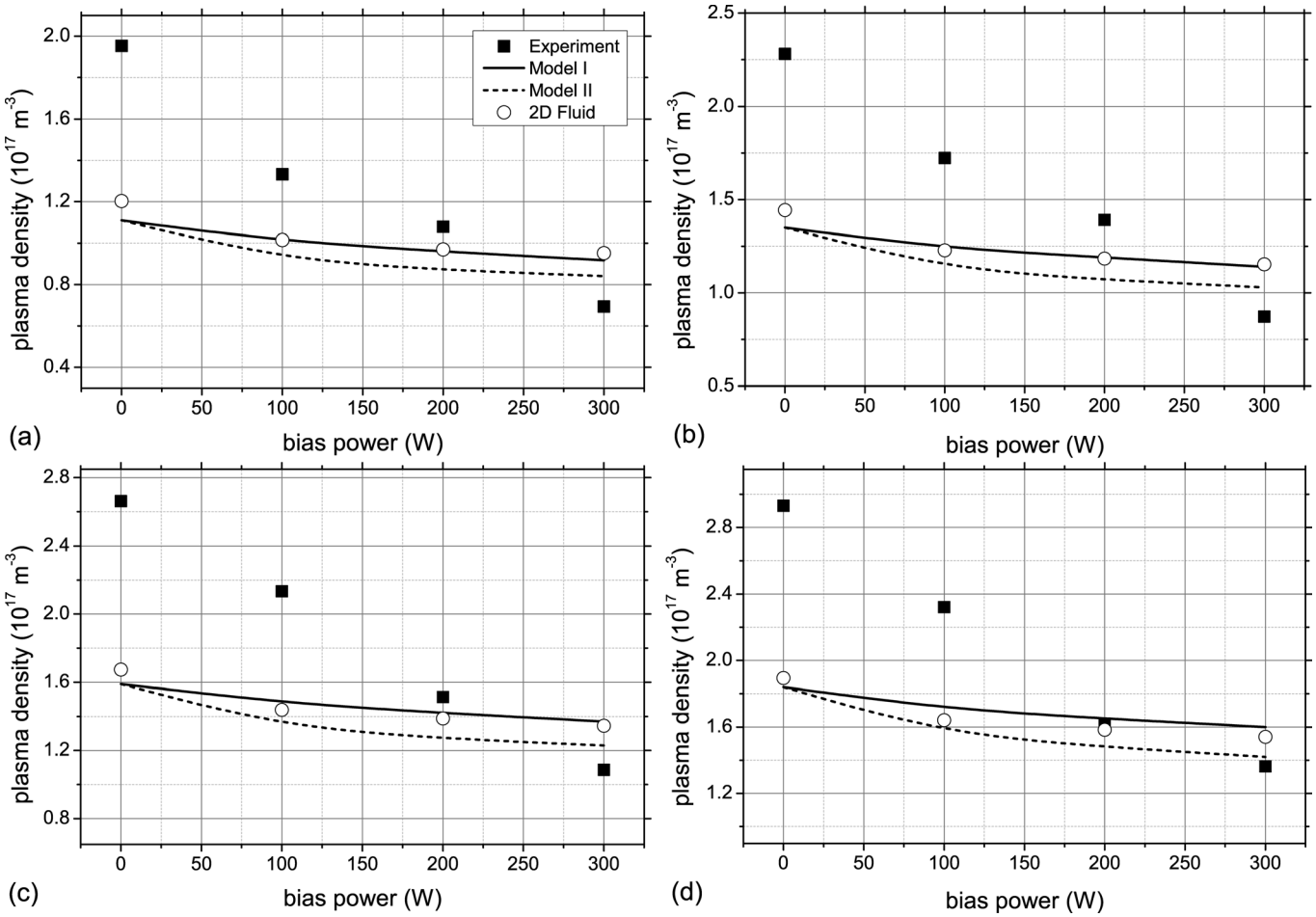

FIG. 4. Dependence of plasma densities on the bias power for various ICP source powers; (a) 500 W, (b) 600 W, (c) 700 W, and (d) 800 W. The (■) is experimental data measured by a cutoff probe, the (◯) is numerically solved data by using a two-dimensional fluid model, and solid and dashed lines are obtained values from Models I and II, respectively.

density decrease with bias power in inductive mode (H mode).

Dependence of the dc self-bias voltage on the bias power for various ICP source powers is shown in Fig. 5. To compare the experimental results, the dc self-bias was defined as one-half of the peak-to-peak voltage.[18] As mentioned in the preceding text, in CFD-ACE +, only the sinusoidal voltage source boundary conditions can be applied for rf bias. Therefore voltage boundary conditions for the two-dimensional fluid simulation were obtained from Model II. We can see that Model I is in a good agreement with measured results. Although there is a difference in the voltage gradient on the bias power in Model II, it is still useful from the point of view of considering the expansibility to two- or three-dimensional simulation. However, there is a difference between the two-dimensional simulation results and measured data.

In numerical results, the differences of the electron density and the self-bias voltage are due to the fact that Model I is the self-consistent fluid model and Model II is the semianalytic model. We can see that the delicate difference of the self-bias voltage can affect the plasma density. It may be curious that numerically solved self-bias voltages are shown to agree well with the experimental results while there is a difference in density gradient on the bias power between numerical and experimental data. This is due to the fact that the plasma density were measured at the chamber center region, although the averaged values of 5 points for the measured electron density were used to compare the simulation results, the averaged values can be high than the plasma density obtained by using the spatially averaged global model. However, the plasma density can be similar with the numerical results near the substrate. Therefore, numerically solved self-bias voltages are shown to agree well with the experimental results.

The dependence of the electron temperature on the bias power at various ICP source powers was solved and presented in Fig. 6. As shown in Fig. 6, the electron temperature decreases little with the source and increases with the bias powers; this is consistent with the previous report of Ref. 17. Our experiments show a slight increase of the electron temperature with bias and source powers as presented in Table II and Fig. 7. Although increase of the electron temperature with source powers is in contradiction to the simulation results, the difference between the results can be negligible within the margin of error. However, as the bias power increases further (>100 W), the electron temperature decreases drastically. This is due to the fact that dominant

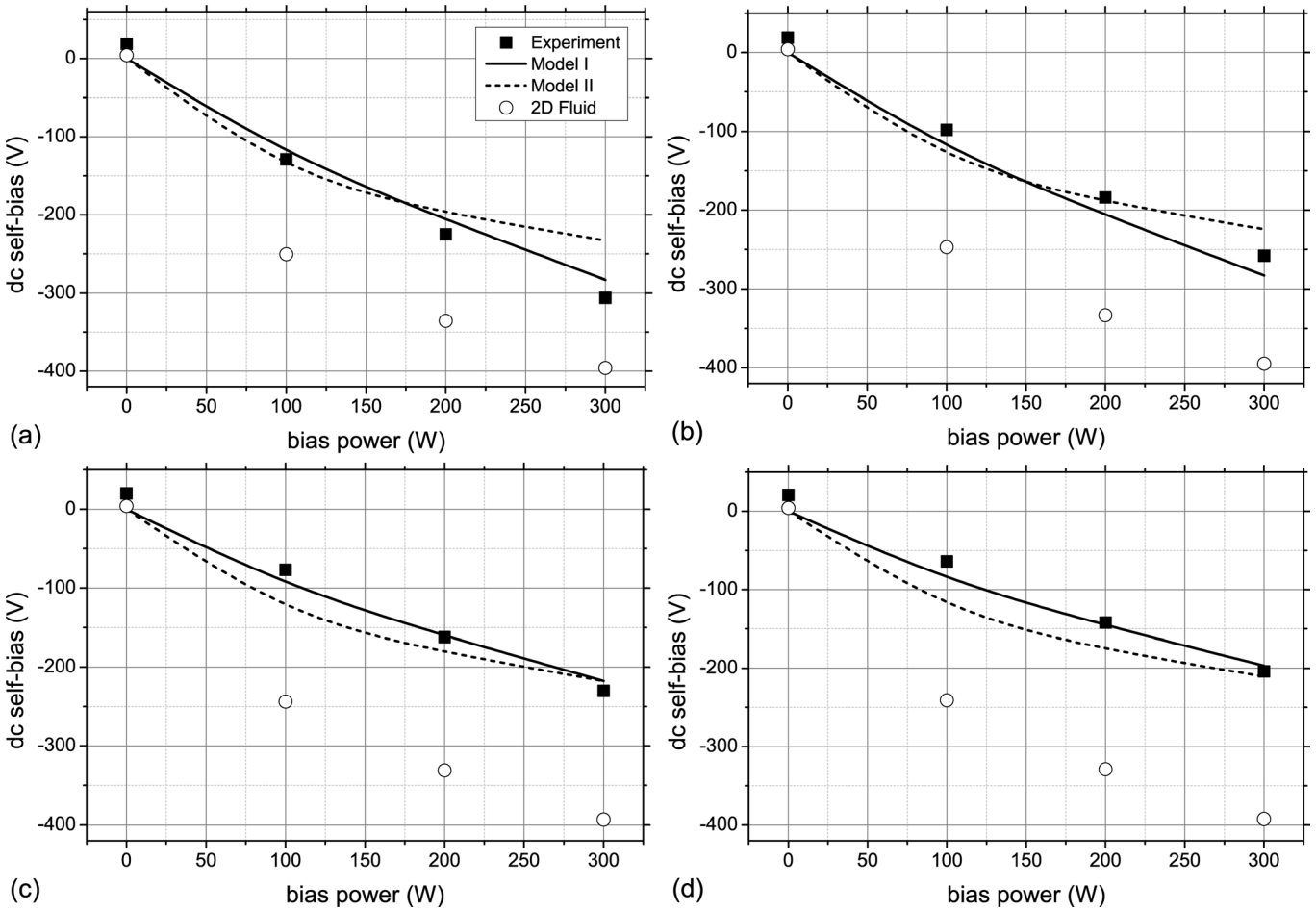

FIG. 5. Dependence of the dc self-bias on the bias power for various ICP source powers; (a) 500 W, (b) 600 W, (c) 700 W, and (d) 800 W. The (■) is experimental data measured by a cutoff probe, the (◯) is numerically solved data by using the two-dimensional fluid model, and solid and dashed lines are obtained values from Models I and II, respectively.

electron heating mechanism of plasma changes from the inductive heating of ICP source power to capacitive heating of bias power while increasing bias power. This change of heating mechanism with bias power is well exhibited in the EEPF evolution from Maxwellian distribution of ICP discharge to bi-Maxwellian distribution of CCP discharge (Fig. 7).[30] Because this electron heating mode transition is of kinetic phenomena in the plasma physics, our model based on the continuum assumption cannot capture this drastic change of the electron temperature with bias power. It is believed that this heating mode change can be easily observed when the capacitive coupling between two antennas (ICP antennas and bias chuck), that is, high voltage (power) and small distance between antennas. This might be a reason why this drastic change of the electron temperature cannot be measured in the previous report[17] with low voltage (power) and long distance between these antennas compared with our experiment.

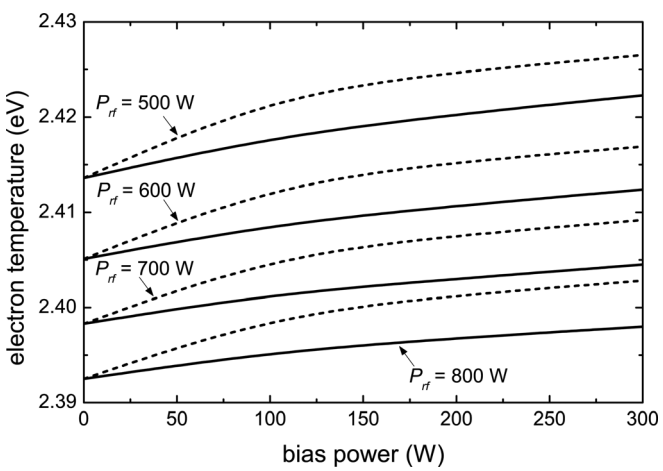

FIG. 6. Dependence of the electron temperature on the bias power for various ICP source powers. Solid and dashed lines are obtained values from Models I and II, respectively.

TABLE II. Measured electron temperatures for various ICP source and bias powers (the reliable electron temperature measurements can not be performed at the bias power of 300 W because of the insufficient rf compensation of Langmuir probe).

	Source power (W)			
Bias power (W)	500	600	700	800
0	2.78	2.84	2.86	2.92
100	2.93	2.93	3.04	2.94
200	0.81	1.02	1.52	1.36
300	—	—	—	—

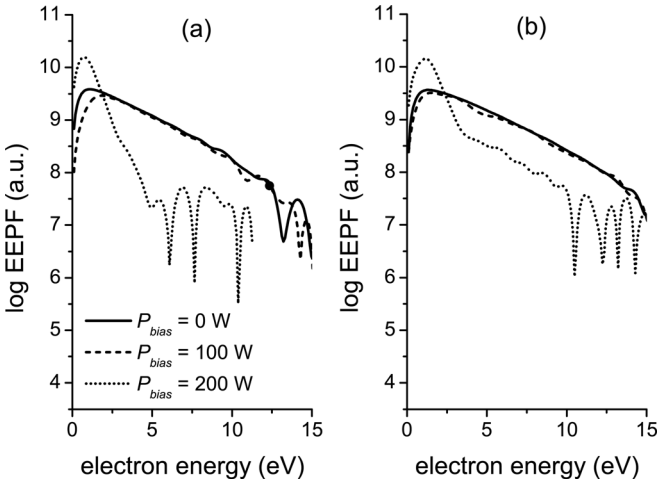

FIG. 7. Measured EEPFs for (a) 500 W and (b) 800 W ICP source powers.

V. CONCLUSIONS

We developed a self-consistent global simulator of solenoidal-type ICP discharges and observed the effect of the rf bias power on the plasma density. We numerically solve a set of spatially averaged fluid equations for charged particles, neutrals, and radicals. Absorbed power by electrons is determined by using an analytic electron heating model including the anomalous skin effect. To analyze the effects of rf bias power on the plasma properties, our model also combines the electron heating and global transport module with an rf sheath module in a self-consistent manner.

To validate our model, experiments were performed in inductively coupled argon plasmas. The simulation results are also compared using the commercial software package CFD-ACE +. We observe that the numerical results are in a good agreement with the experimental results, and dependence of the electron density on the bias power cannot be negligible.

In our work, we assumed that the time averaged power flowing from the rf bias power into the discharge is totally absorbed within the sheath region. However, power flowing from the rf bias power into the discharge could not be negligible under the other conditions. Therefore we will develop a model including the stochastic and ohmic heating effect. This is under active study and will be reported later.

ACKNOWLEDGMENTS

We are grateful to Prof. N. S. Yoon for his helpful comments on this work.

[1]N. S. Yoon, S. S. Kim, C. S. Chang, and D. I. Choi, Phys. Rev. E **54**, 757 (1996).
[2]N. S. Yoon, S. M. Hwang, and D. I. Choi, Phys. Rev. E **55**, 7536 (1997).
[3]K. I. You and N. S. Yoon, Phys. Rev. E **59**, 7074 (1999).
[4]S. S. Kim, S. Hamaguchi, N. S. Yoon, C. S. Chang, Y. D. Lee, and S. H. Ku, Phys. Plasmas **8**, 1384 (2001).
[5]D. C. Kwon, N. S. Yoon, J. H. Kim, Y. H. Shin, and K. H. Chung, J. Korean Phys. Soc. **47**, 163 (2005).
[6]D. C. Kwon, N. S. Yoon, J. H. Kim, Y. H. Shin, and K. H. Chung, J. Korean Phys. Soc. **50**, 40 (2007).
[7]M. A. Lieberman, IEEE Trans. Plasma Sci. **16**, 638 (1988).
[8]M. A. Lieberman, IEEE Trans. Plasma Sci. **17**, 338 (1989).
[9]V. A. Godyak and N. Stenberg, IEEE Trans. Plasma Sci. **18**, 159 (1990).
[10]V. A. Godyak and N. Stenberg, Phys. Rev. A **42**, 2299 (1990).
[11]P. A. Miller and M. E. Riley, J. Appl. Phys. **82**, 3689 (1997).
[12]T. Panagopoulos and D. J. Economou, J. Appl. Phys. **85**, 3435 (1999).
[13]E. A. Edelberg and E. S. Aydil, J. Appl. Phys. **86**, 4799 (1999).
[14]D. Bose, T. R. Govindan, and M. Meyyappan, J. Appl. Phys. **87**, 7176 (2000).
[15]Z. L. Dai, Y. N. Wang, and T. C. Ma, Phys. Rev. E **65**, 036403 (2002).
[16]M. J. Grapperhaus and M. J. Kushner, J. Appl. Phys. **81**, 569 (1997).
[17]H. C. Lee, M. H. Lee, and C. W. Chung, Appl. Phys. Lett. **96**, 071501 (2010).
[18]M. A. Lieberman and A. J. Lichtenberg, *Principle of Plasma Discharges and Materials Processing*, 2nd ed. (Wiley, New York, 2004).
[19]N. S. Yoon, S. S. Kim, C. S. Chang, and D. I. Choi, J. Korean Phys. Soc. **28**, 172 (1995).
[20]J.-H. Kim. S.-C. Choi, Y.-H. Shin, and K.-H. Chung, Rev. Sci. Instrum. **75**, 2706 (2004).
[21]M. A. Sobolewski and J.-H. Kim. J. Appl. Phys. **102**, 113302 (2007).
[22]S. J. You, S. S. Kim, and H. Y. Chang, Appl. Phys. Lett. **85**, 4872 (2004).
[23]S. J. You, S. S. Kim, J. H. Kim, D. J. Seong, Y. H. Shin, and H. Y. Chang, Appl. Phys. Lett. **91**, 221501 (2007).
[24]http://www.esi-cfd.com. for information on the commercial software package cfd-ace +.
[25]A. Metze, D. W. Ernie, and H. J. Oskam, J. Appl. Phys. **60**, 3081 (1986).
[26]M. Hayashi, Nagoya Institute of Technology Report, No. IPPJ-AM-19 (1991).
[27]D. Rapp and P. Englander-Golden, J. Chem. Phys. **43**, 1464 (1965).
[28]S. Tinck, W. Boullart, and A. Bogaerts, J. Phys. D **41**, 065207 (2008).
[29]A. V. Vasenkov, X. Li, G. S. Oehrlein, and M. J. Kushner, J. Vac. Sci. Technol. A **22**, 511 (2004).
[30]V. A. Godyak and R. B. Piejak, Phys. Rev. Lett. **65**, 996 (1990).